Simulation of complex plasmonic circuits including bends

Claudio Dellagiacoma,[1] **Theo Lasser,**[1] **Olivier J. F. Martin,**[1,3,5]
Aloyse Degiron,[2] **Jack J. Mock,**[2] **and David R. Smith**[2,4,6]

[1]*Institut de Microtechnique*
Swiss Federal Institute of Technology Lausanne (EPFL)
1015 Lausanne, Switzerland
[2]*Department of Electrical and Computer Engineering*
Duke University
Durham, NC 27708, USA
[3]*olivier.martin@epfl.ch*
[4]*drsmith@duke.edu*
[5]*http://www.nanophotonics.ch*
[6]*http://people.ee.duke.edu/~drsmith*

Abstract: Using a finite-element, full-wave modeling approach, we present a flexible method of analyzing and simulating dielectric and plasmonic waveguide structures as well as their mode coupling. This method is applied to an integrated plasmonic circuit where a straight dielectric waveguide couples through a straight hybrid long-range plasmon waveguide to a uniformly bent hybrid one. The hybrid waveguide comprises a thin metal core embedded in a two–dimensional dielectric waveguide. The performance of such plasmonic circuits in terms of insertion losses is discussed.

OCIS codes: (250.5300) Photonic integrated circuits; (250.5403) Plasmonics; (250.5460) Polymer waveguides.

References and links

1. M. Hochberg, T. Baehr-Jones, C. Walker, and A. Scherer, "Integrated plasmon and dielectric waveguides," Opt. Express **12**, 5481–5486 (2004).
2. A. Degiron, S.-Y. Cho, T. Tyler, N. M. Jokerst, and D. R. Smith, "Directional coupling between dielectric and long-range plasmon waveguides," N. J. Phys. **11**, 015002 (2009).
3. P. Berini, R. Charbonneau, and N. Lahoud, "Long-range surface plasmons on ultrathin membranes," Nano Lett. **7**, 1376–1380 (2007).
4. R. Buckley and P. Berini, "Radiation suppressing metallo-dielectric optical waveguides," J. Lightwave Technol. **27**, 2800–2808 (2009).
5. R. Buckley and P. Berini, "Long-range substantially nonradiative metallo-dielectric waveguide," Opt. Lett. **34**, 223–225 (2009).
6. P. Berini and R. Buckley, "On the convergence and accuracy of numerical mode computations of surface plasmon waveguides," J. Comput. Theor. Nanosci. **6**, 2040–2053 (2009).
7. A. Degiron, S.-Y. Cho, C. Harrison, N. M. Jokerst, C. Dellagiacoma, O. J. F. Martin, and D. R. Smith, "Experimental comparison between conventional and hybrid long-range surface plasmon waveguide bends," Phys. Rev. A **77**, 021804 (2008).
8. A. Krasavin, P. Bolger, A. Zayats, Stær, T. Holmgaard, Z. Chen, S. Bozhevolnyi, L. Markey, and A. Dereux, "Active components for integrated plasmonic circuits," in "2nd IEEE LEOS Winter Topicals, WTM 2009," (2009).
9. T. J. Davis, K. C. Vernon, and D. E. Gomez, "A plasmonic "ac wheatstone bridge" circuit for high-sensitivity phase measurement and single-molecule detection," J. Appl. Phys. **106**, 043502 (2009).
10. Y.-J. Tsai, A. Degiron, N. M. Jokerst, and D. R. Smith, "Plasmonic multi-mode interference couplers," Opt. Express **17**, 17471–17482 (2009).

#144920 - $15.00 USD Received 28 Mar 2011; revised 21 Aug 2011; accepted 28 Aug 2011; published 15 Sep 2011

11. P. Berini, "Bulk and surface sensitivities of surface plasmon waveguides," N. J. Phys. **10**, 105010 (2008).
12. R. Charbonneau, M. Tencer, N. Lahoud, and P. Berini, "Demonstration of surface sensing using long-range surface plasmon waveguides on silica," Sens. Actuators B Chem. **134**, 455–461 (2008).
13. A. Degiron and D.R. Smith, "Numerical simulations of long-range plasmons," Opt. Express **14**, 1611–1625 (2006).
14. R. Buckley and P. Berini, "Figures of merit for 2D surface plasmon waveguides and application to metal stripes," Opt. Express **15**, 12174–12182 (2007).
15. A. Degiron, C. Dellagiacoma, J. G. McIlhargey, G. Shvets, O. J. F. Martin, and D. R. Smith, "Simulations of hybrid long-range plasmon modes with application to 90 degrees bends," Opt. Lett. **32**, 2354–2356 (2007).
16. R. Soref, "The past, present, and future of silicon photonics," IEEE J. Sel. Top. Quantum Electron. **12**, 1678–1687 (2006).
17. C. Wang and L. Lin, "Nanoscale waveguiding methods," Nanoscale Res. Lett. **2**, 219–229 (2007).
18. M. Mastro, R. Holm, C. E. Jr, and J. Kim, "Electromagnetic propagation in nanostructures," J. Ceram. Proc. Res. **9**, 1–5 (2008).
19. J. T. Kim, J. J. Ju, S. Park, M. su Kim, S. K. Park, and M.-H. Lee, "Chip-to-chip optical interconnect using gold long-range surface plasmon polariton waveguides," Opt. Express **16**, 13133–13138 (2008).
20. J. Ctyroky, J. Homola, and M. Skalsky, "Modelling of surface plasmon resonance waveguide sensor by complex mode expansion and propagation method," Opt. Quantum Electron. **29**, 301–311 (1997).
21. J. Shibayama, T. Yamazaki, J. Yamauchi, and H. Nakano, "Eigenmode analysis of a light-guiding metal line loaded on a dielectric substrate using the imaginary-distance beam-propagation method," J. Lightwave Technol. **23**, 1533–1539 (2005).
22. P. Berini and J. Lu, "Curved long-range surface plasmon-polariton waveguides," Opt. Express **14**, 2365–2371 (2006).
23. Y.-C. Lu, L. Yang, W.-P. Huang, and S.-S. Jian, "Improved full-vector finite-difference complex mode solver for optical waveguides of circular symmetry," J. Lightwave Technol. **26**, 1868–1876 (2008).
24. S. Burger, L. Zschiedrich, J. Pomplun, and F. Schmidt, "Jcmsuite: An adaptive fem solver or precise simulations in nano-optics," in "Integrated Photonics and Nanophotonics Research and Applications," (Optical Society of America, 2008), paper ITuE4.
25. G. C. des Francs, J. Grandidier, S. Massenot, A. Bouhelier, J.-C. Weeber, and A. Dereux, "Integrated plasmonic waveguides: A mode solver based on density of states formulation," Phys. Rev. B **80**, 115419 (2009).
26. *COMSOL Multiphysics User Guide, Version 3.3* (COMSOL AB, Stockholm, Sweden, 2006).
27. P. Bienstman, E. Six, M. Roelens, M. Vanwolleghem, and R. Baets, "Calculation of bending losses in dielectric waveguides using eigenmode expansion and perfectly matched layers," IEEE Photon. Technol. Lett. **14**, 164–166 (2002).
28. M. Paulus, P. Gay-Balmaz, and O. J. F. Martin, "Accurate and efficient computation of the green's tensor for stratified media," Phys. Rev. E Stat. Phys. Plasmas Fluids Relat. Interdiscip. Topics **62**, 5797–5807 (2000).
29. M. Paulus and O. J. F. Martin, "How to tap an innocent waveguide," Opt. Express **8**, 644–648 (2001).
30. M. Paulus and O. J. F. Martin, "A green's tensor approach to the modeling of nanostructure replication and characterization," Radio Sci. **38**, 8024 (2003).
31. R. J. Deri and E. Kapon, "Low-loss iii-v semiconductor optical waveguides," IEEE J. Quantum Electron. **27**, 626–640 (1991).
32. J. Jin, *The Finite Element Method in Electromagnetics*, 2nd ed. (John Wiley and Sons, 2002).
33. M. Heiblum and J. Harris, "Analysis of curved optical waveguides by conformal transformation," IEEE J. Quantum Electron. **QE11**, 75–83 (1975).
34. T. Yamamoto and M. Koshiba, "Numerical analysis of curvature loss in optical waveguides by the finite-element method," J. Lightwave Technol. **11**, 1579–1583 (1993).
35. K. Kakihara, N. Kono, K. Saitoh, and M. Koshiba, "Full-vectorial finite element method in a cylindrical coordinate system for loss analysis of photonic wire bends," Opt. Express **14**, 11128–11141 (2006).
36. W. Lui, C. Xu, T. Hirono, K. Yokoyama, and W. Huang, "Full-vectorial wave propagation in semiconductor optical bending waveguides and equivalent straight waveguide approximations," J. Lightwave Technol. **16**, 910–914 (1998).
37. S. Lidgate, P. Sewell, and T. Benson, "Conformal mapping: limitations for waveguide bend analysis," IEE Proc.: Sci., Meas. Technol. **149**, 262–266 (2002).
38. Y. Tsuji and M. Koshiba, "Finite element method using port truncation by perfectly matched layer boundary conditions for optical waveguide discontinuity problems," J. Lightwave Technol. **20**, 463–468 (2002).
39. X. Heng, X. Cui, D. W. Knapp, J. Wu, Z. Yaqoob, E. J. McDowell, D. Psaltis, and C. Yang, "Characterization of light collection through a subwavelength aperture from a point source," Opt. Express **14**, 10410–10425 (2006).
40. W. C. Chew, J. M. Jin, and E. Michielssen, "Complex coordinate stretching as a generalized absorbing boundary condition," Microw. Opt. Technol. Lett. **17-21** (1997).
41. F. Teixeira and W. Chew, "Systematic derivation of anisotropic pml absorbing media in cylindrical and spherical coordinates," IEEE Microw. Guid. Wave Lett. **7**, 371–373 (1997).
42. D. Marcuse, *Theory of Dielectric Optical Waveguides* (Academic Press, 1974), p. 267.

#144920 - $15.00 USD Received 28 Mar 2011; revised 21 Aug 2011; accepted 28 Aug 2011; published 15 Sep 2011

43. R. Charbonneau, C. Scales, I. Breukelaar, S. Fafard, N. Lahoud, G. Mattiussi, and P. Berini "Passive integrated optics elements based on long-range surface plasmon polaritons," J. Lightwave Technol. **24**, 477–494 (2006).
44. P. Johnson and R. Christy, "Optical constants of the noble metals," Phys. Rev. B **6**, 4370–4379 (1972).
45. T. Nikolajsen, K. Leosson, I. Salakhutdinov, and S. Bozhevolnyi, "Polymer-based surface-plasmon-polariton stripe waveguides at telecommunication wavelengths," Appl. Phys. Lett. **82**, 668–670 (2003).
46. Q. Min, C. Chen, P. Berini, and R. Gordon, "Long range surface plasmons on asymmetric suspended thin film structures for biosensing applications," Opt. Express **18**, 19009–19019 (2010).
47. P. Berini, R. Charbonneau, N. Lahoud, and G. Mattiussi, "Characterization of long–range surface–plasmon–polariton waveguides," J. Appl. Phys. **98**, 043109 (2005).

1. Introduction

Over the past ten years, tremendous developments have occurred in the field of surface plasmon polaritons (SPPs)-propagating electromagnetic waves at a dielectric–metal interface [1–7]. The strong confinement and local field enhancement associated with SPPs enables them to resolve spatial detail beyond the diffraction limit. For this reason, SPPs have become widely appreciated for their potential to create extremely compact optical devices with highly confined electric fields [8–12]. However, since at optical wavelengths metals are strongly absorbing, there is a trade–off between the field confinement and the absorption losses [13, 14]. Hence, the long propagation distances that can be achieved using so–called long–range SPP modes (LRSPPs) on thin metal films or metal strips correlate with weak confinement, having similar properties to dielectric waveguides. Hybrid SPPs can relax this constraint by combining LRSPPs with a two–dimensional dielectric waveguide, increasing the field confinement further by total internal reflection [15]. Similarly, curved hybrid LRSPP metal strips reach smaller radii than non hybrid ones for the same total bending loss, even with only two–dimensional dielectric waveguides [7]. This might be desirable for integrated optical circuits [16–19].

Simulation techniques are essential for the design and practical implementation of such photonic circuits based on plasmonic waveguides. In this paper, we present a versatile numerical simulation approach for straight and curved SPP waveguides, based on the commercial finite element software Comsol. In the following, this powerful tool is first applied to the simulation of coupling from an integrated dielectric waveguide to a straight LRSPP waveguide. In particular, the geometrical parameters are optimized for best transmission. Next, the coupling from the latter straight SPP waveguide to a curved one is studied. The geometrical parameters of the curved SPP waveguide are found such that different optimal bending radii are obtained. In order to improve the coupling efficiency, the horizontal and vertical offsets of the waveguides are analyzed. Conclusions are drawn on the complete structure including bends and coupling from conventional waveguides to plasmonic ones, as illustrated in Fig. 1.

2. Simulation method

The structure of interest is shown in Fig. 1; the metal strips have thicknesses of $t = 10 \ldots 35\,\mathrm{nm}$, widths in the range $w = 1 \ldots 10\,\mu\mathrm{m}$ and are several millimeters long; they are embedded in an isotropic dielectric material. The straight and uniformly bent rectangular waveguides considered here can be fully characterized by modeling their cross–section since their geometrical parameters as well as their mode properties do not change along the direction of propagation. Therefore, 2D calculations can be performed, significantly reducing the computational effort. A variety of techniques have been used to compute the eigenmodes supported by plasmonic waveguides [13, 20–25]. The results presented here are obtained with the Comsol implementation of the finite elements method [26]. This platform offers great flexibility and is widely used in engineering. The eigenmodes associated with straight plasmonic waveguides can be computed easily by simply defining the geometry of the cross-section and using the complex permittivity of the metal. Typically, about $10'000$ mesh points are used to discretize the geom-

#144920 - $15.00 USD Received 28 Mar 2011; revised 21 Aug 2011; accepted 28 Aug 2011; published 15 Sep 2011

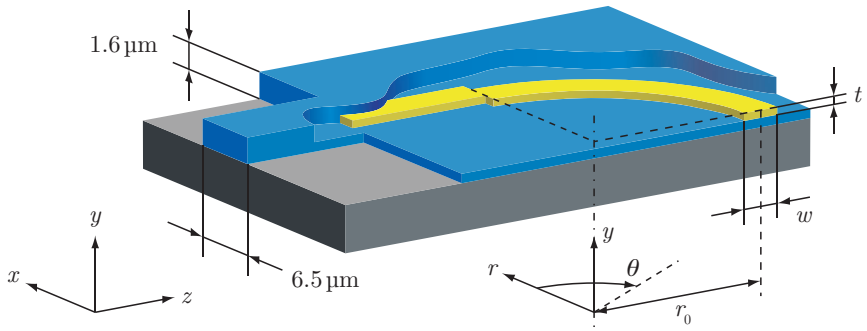

Fig. 1. Illustration of the considered dielectric and plasmonic waveguide structure. Modes couple from a dielectric waveguide (BCB on SiO_2) over a straight to a uniformly bent hybrid plasmonic waveguide (Au core embedded in BCB on SiO_2).

etry, with a higher refinement required within the metal and in the immediate vicinity to its surfaces. This corresponds to typically 100 meshes per vacuum wavelength in the metal and 10 per vacuum wavelength in the dielectric. The size of the computation window is typically $60\,\mu\text{m} \times 10\,\mu\text{m}$. A higher mesh density up to about 100′000 meshes was required for computation of the coupling efficiency.

The peculiarities of plasmonic waveguides require however to pay special attention to the boundary conditions, which must be chosen carefully [27]. Note that this is not the case for alternative techniques such as the Green's tensor technique [25, 28–30]. For the straight waveguides, the fundamental LRSPP mode which is of interest in this study is non–radiative and bound to the metal structure. In this case a variety of boundary conditions can be used, provided that they are placed far enough from the structure to leave the SPP modes unperturbed. We chose a combination of perfect electric and perfect magnetic walls located 40 µm away from the structure. More complex boundary conditions would needlessly complicate the computation in this case.

On the other hand, for bent plasmonic waveguides, all the modes are radiative as is the case for curved dielectric waveguides [31]. This significantly complicates the calculation since energy must now be allowed to escape from the computation window without being reflected back. This is achieved by placing perfectly matched layers (PMLs) at the boundaries of the computation window [32].

Bent geometries can either be modeled using a conformal transformation to obtain an equivalent straight waveguide [27, 33], or the wave equations can be directly solved using a cylindrical coordinate system [34, 35]. In the equivalent straight waveguide formulation, the curved waveguide is transformed into an equivalent straight one using a conformal mapping of the index profile $n \mapsto n_t$:

$$n_t = n \exp \frac{u}{r_0} \quad \text{and} \quad u = r_0 \ln \frac{r}{r_0}, \tag{1}$$

where r_0 is the radius of curvature and u is the transformed coordinate corresponding to r. Conventional numerical techniques can then be used to simulate the equivalent straight waveguide. A drawback of this approach lies in the increasing refractive index for large r, which complicates the boundary conditions at this edge of the computation window, leading to unreliable numerical results for small radii of curvature r_0 [36, 37].

To avoid these difficulties, we chose to solve the wave equation directly in cylindrical coordinates. However, since Comsol uses only Cartesian coordinates, we will keep in the following the x, y, and z symbols to facilitate the replication of our work. Hence, for curved geometries,

#144920 - $15.00 USD Received 28 Mar 2011; revised 21 Aug 2011; accepted 28 Aug 2011; published 15 Sep 2011

the x–coordinate represents the direction of the radius and z the angular direction θ (see Fig. 1).

Since Comsol does not support eigenmode analysis in cylindrical coordinates, the weak form of the eigenmode solver in Cartesian coordinates must be modified to handle cylindrical coordinates. This is achieved by multiplying the volume and surface elements of the integrals by r and by replacing the definition of the curl operator with

$$\nabla \times \begin{pmatrix} E_x \\ E_y \\ -\alpha e_z \end{pmatrix} e^{\alpha r_0 \theta} = \begin{pmatrix} -\alpha \left(\frac{r_0}{r} E_y + \frac{\partial e_z}{\partial y} \right) \\ \alpha \frac{1}{r} \left(e_z + r \frac{\partial e_z}{\partial x} + r_0 E_x \right) \\ \frac{\partial E_y}{\partial x} - \frac{\partial E_x}{\partial y} \end{pmatrix} e^{\alpha r_0 \theta}, \tag{2}$$

when solving for the electric field. In Equation (2) $\beta = -j\alpha$ is the propagation constant and α the corresponding eigenvalue of the problem [26].

For the boundary conditions, the uniform PMLs provided by Comsol appeared to be insufficient and produced noticeable reflections at the edges of the computation window, thereby influencing the simulation results. Hence anisotropic cylindrical PMLs with gradual absorption have been implemented to obtain accurate results [32]. Accordingly, the material properties of a PML adjoining a computational domain with given permittivity ε and permeability μ becomes

$$[\varepsilon]_{\mathrm{PML}} = \varepsilon [\Lambda] \quad \text{and} \quad [\mu]_{\mathrm{PML}} = \mu [\Lambda], \tag{3}$$

with

$$[\Lambda] = \begin{bmatrix} \frac{s_\theta s_y}{s_r} & 0 & 0 \\ 0 & \frac{s_y s_r}{s_\theta} & 0 \\ 0 & 0 & \frac{s_r s_\theta}{s_y} \end{bmatrix}. \tag{4}$$

The complex values s_r, s_θ and s_y introduce absorption analytically without creating reflections at the interface between the computation domain and the PML. In order to minimize the remaining numerical reflections, a progressive absorption profile was used [32, 38–40]:

$$s_r = 1 + j \left(\frac{r - r_b}{L} \right)^2 \delta_{max}, \tag{5}$$

where L is the thickness and r_b the starting point of the PML. An optimal thickness was found to be 1 to 2 transverse wavelengths of the corresponding mode. At the same time, it is important to use in the order of 10 finite elements per wavelength — not only in the PML, but over the entire radiation region — to prevent distortion of the modes. The maximal absorption reached at the end of the PML was chosen as $\delta_{max} = 2$, in good agreement with the literature [40].

Since the PML is cylindrical, s_θ and s_y in Eq. (4) become:

$$\begin{cases} s_\phi & = \frac{\widetilde{r}}{r} \\ s_y & = 1, \end{cases} \qquad \text{with} \quad \widetilde{r} = r_b \int_{r_b}^{r} s_r(r')\, dr', \tag{6}$$

as explained in detail in Ref. [41].

2.1. Mode coupling

The aim of this paper is to simulate complex circuits that include several plasmonic waveguides, hence the transmission from one waveguide to the next one must be calculated. This mode coupling analysis relies on overlap integrals of the electric field distributions [42]. Since all the

#144920 - $15.00 USD Received 28 Mar 2011; revised 21 Aug 2011; accepted 28 Aug 2011; published 15 Sep 2011

considered modes are transverse magnetic like, the x–component of the electric field can be neglected. Therefore the coupling coefficient C can be written as

$$C = \frac{\iint_{\Omega} E_{y_1} E_{y_2}^* \, d\Omega}{\sqrt{\iint_{\Omega} E_{y_1} E_{y_1}^* \, d\Omega \iint_{\Omega} E_{y_2} E_{y_2}^* \, d\Omega}} . \tag{7}$$

The corresponding coupling loss is

$$\alpha_C = -20 \log |C| . \tag{8}$$

Slightly different propagation constants as well as the partial overlap of the field distribution can cause coupling losses by reflection. As long as those reflections are small, the approximation (7) is good and the wave vector mismatch can be neglected [42]. Moreover, the normalization applied in Eq. (7) is not rigorously correct due to the radiation. However, since the computation domain is limited and the radiation small compared to the guided field, Eq. (7) remains a good approximation for the system under study [43].

3. Results and discussion

All the results presented here are computed for the free space wavelength $\lambda = 1.55\,\mu$m. The plasmonic waveguides are made of gold with permittivity $\varepsilon_{Au} = -131.95 + 14.5j$ [44]. Benzocyclobutene (BCB, $n_{BCB} = 1.535$ [45]) is used as dielectric material and SiO_2 as substrate ($n_{SiO2} = 1.44$).

The integration of plasmonic circuits requires the coupling from a conventional integrated dielectric waveguide to a hybrid LRSPP waveguide. The considered dielectric waveguide is made of a BCB strip in air on a SiO_2 substrate. The hybrid LRSPP single mode waveguide is a 20 nm thin, 3 µm wide Au strip embedded in a BCB layer. This BCB layer and the dielectric waveguide have the same thickness of 1.6 µm. In order to achieve efficient coupling, the dielectric waveguide width has to be larger than 3 µm because of the broad field distribution of the

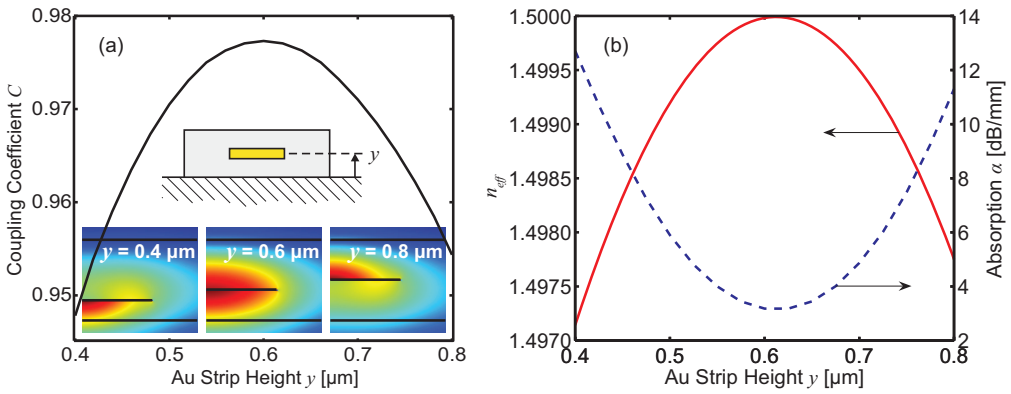

Fig. 2. Coupling from a 6.5 µm wide and 1.6 µm thick dielectric waveguide to a hybrid plasmonic guide: (a) Coupling efficiency and (b) effective index and absorption of the plasmonic waveguide as a function of the Au strip position within the two–dimensional dielectric waveguide. The center is at $y = 0.8\,\mu$m. The dimensions of the Au strip are $3\,\mu\text{m} \times 20\,\text{nm}$. The inset in (a) shows the electric field amplitude distribution for three different y–positions of the plasmonic waveguide.

#144920 - $15.00 USD Received 28 Mar 2011; revised 21 Aug 2011; accepted 28 Aug 2011; published 15 Sep 2011

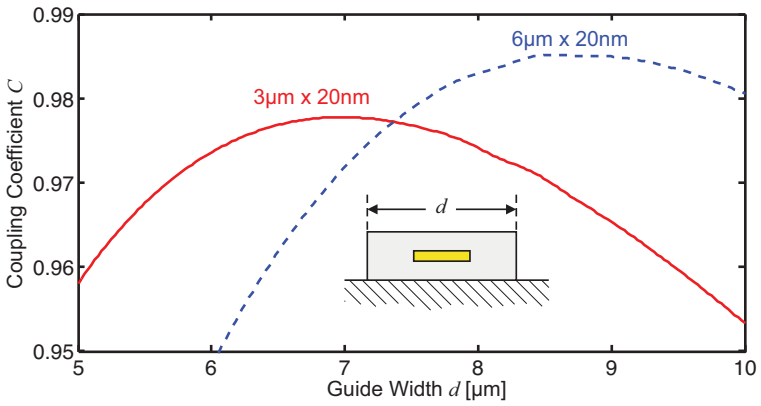

Fig. 3. Coupling from a 1.6 µm thick dielectric waveguide to a hybrid plasmonic one: coupling efficiency as a function of the dielectric waveguide width for a plasmonic waveguide located at the optimal height. Two different Au strips are investigated, with dimensions 3 µm × 20 nm and 6 µm × 20 nm, respectively.

plasmonic waveguide. We consider a 6.5 µm wide integrated dielectric waveguide for optimal coupling (cf. Fig. 3). By means of a taper, this multimode dielectric waveguide can easily be excited by a single mode integrated dielectric waveguide or a dielectric fiber.

Let us first consider the coupling from the dielectric waveguide to the straight plasmonic waveguide, Fig. 2. The field distribution associated with the LRSPP mode strongly depends on the position of the Au strip within the BCB background layer, as shown in the inset of panel (a), where the field is computed for three different vertical positions of the Au strip. Hence, the coupling efficiency between the fundamental mode of the dielectric waveguide and the LRSPP mode in the BCB layer depends on the position of the Au strip within the structure. The more symmetric the LRSPP mode, the better the coupling efficiency. Clearly, the best coupling efficiency does not correspond to the center position (0.8 µm), but is shifted towards the high refractive index substrate, Fig. 2(a).

Changing the Au strip position within the BCB background also influences the propagation characteristics of the LRSPP mode. Figure 2(b) shows the real part of the effective mode index and the propagation loss as a function of the Au strip position. Here it indicates that a more symmetric field distribution decreases the propagation losses. In this regard, we point out that the result is a general trend for asymmetric multilayer structures, as numerically predicted by Berini in Ref. [46]. The optimum for coupling and propagation losses is found for a strip position $y \simeq 0.6\,\mu$m.

Using this Au strip position $y = 0.6\,\mu$m, one can find the optimal dielectric waveguide width which provides the best coupling efficiency. Figure 3 indicates that a width of 6.5 µm produces the best coupling efficiency with very low losses of about 0.1 dB.

Waveguide bends are essential for the design of integrated plasmonic circuits. As previously investigated by Berini *et al.*, an optimal radius r_{opt} for a given plasmonic waveguide exists, where the radiation and absorption losses are minimized [22]. Recently, it was shown that hybrid plasmonic waveguides embedded in a dielectric layer allow to reduce r_{opt} further [15]. This is illustrated in Fig. 4, which gives the optimal radii and the corresponding bending losses as a function of the plasmonic waveguide geometry. Note that the minimum optimal radius is barely less than half a millimeter for a 35 nm thick waveguide. For a given thickness, the optimal radius *and* the minimal bending losses can be reduced by increasing the metal strip width, up to about 11 µm. Figure 5 indicates the minimal bending losses for a waveguide width of 2. . . 11 µm

#144920 - $15.00 USD Received 28 Mar 2011; revised 21 Aug 2011; accepted 28 Aug 2011; published 15 Sep 2011

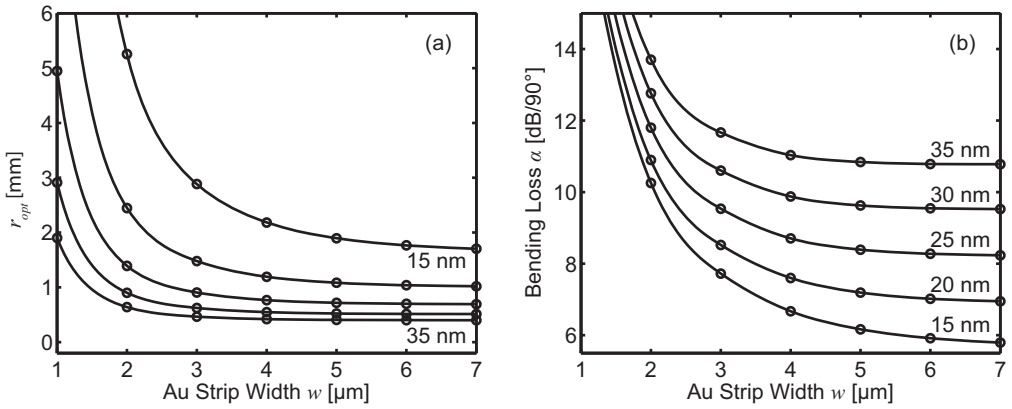

Fig. 4. Characteristics of bent hybrid plasmonic waveguides: (a) optimal radius and (b) corresponding minimal bending loss as a function of the Au strip width w and thickness ($t = 15 \ldots 35\,\mathrm{nm}$).

at a specific bending radius. The radii correspond to the optimal radii of the respective strip width and thickness as shown in Fig. 4. The bending loss decreases until about a width of 11 µm, but it increases strongly for radii smaller than about 1 mm. As long as the fabrication permits a smooth Au strip surface, the thinner the waveguide the smaller the absorption; but such a thin structure requires a large curvature radius. Accordingly, thin but wide Au strips of $\approx 10\,\mu\mathrm{m}$ yield the lowest bending losses. However, it should be pointed out that such a wide bend is a multimode structure and different modes are generally not orthogonal for the curved geometry. In other words, even if only the fundamental mode is launched at the bend input, higher order modes will inevitably be excited as the signal propagates along the bend.

Let us now consider the junction between a straight and a curved plasmonic waveguide. The straight waveguide has the same dimensions as previously ($3\,\mu\mathrm{m} \times 20\,\mathrm{nm}$), whereas the 3 µm wide curved waveguide has a thickness such that the desired radius is optimal. As proposed in

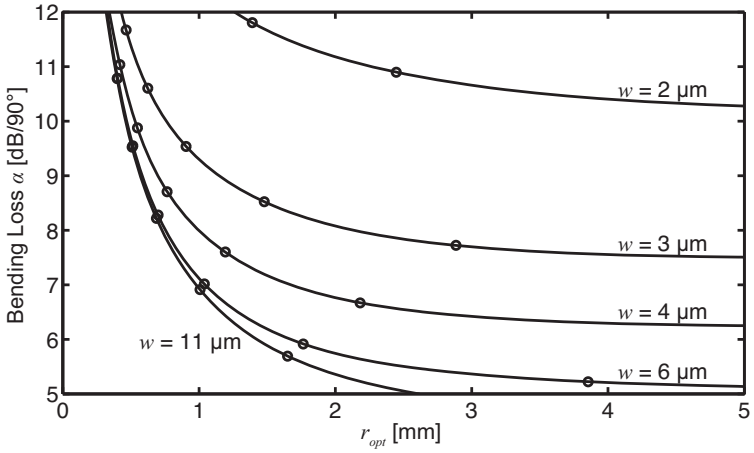

Fig. 5. Minimal bending loss for a 2, 3, 4, 6 and 11 µm wide Au strip as a function of the bending radius. The radii correspond to the optimal radii of the respective strip width and thickness as represented in Fig. 4.

#144920 - $15.00 USD Received 28 Mar 2011; revised 21 Aug 2011; accepted 28 Aug 2011; published 15 Sep 2011

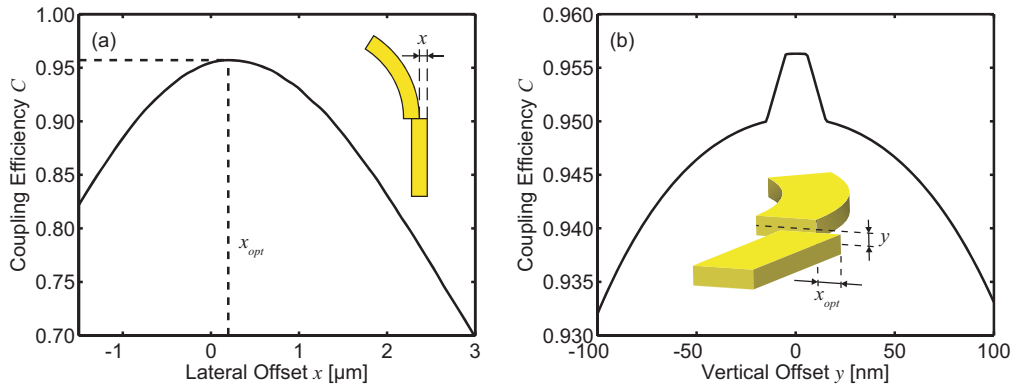

Fig. 6. Lateral and vertical offset between a straight and bent hybrid waveguide: Coupling efficiency as a function (a) of the lateral offset and (b) of the vertical offset. The Au strips of the straight and bent waveguide are 3 µm × 20 nm and 3 µm × 10 nm, respectively.

[22] and applied for dielectric waveguides, the coupling efficiency can be improved by laterally offseting the curved waveguide towards the center. Figure 6(a) shows the coupling efficiency as a function of the lateral offset. Here, the coupling between a 20 nm thick straight waveguide and a 10 nm thick bend with a radius $r_0 = r_{opt} = 8$ mm is considered. We acknowledge that even if this configuration is favorable in terms of coupling losses, it would be technically difficult to fabricate because the metal thickness varies between the straight and the bend waveguide. In addition, achieving a smooth 10 nm thick bend using standard metal deposition techniques appears challenging because evaporated metallic films are typically not smooth for thicknesses smaller than 20 nm or so [47]. Since the straight and the curved waveguide do not have the same thickness in this case, the coupling efficiency as a function of a vertical offset must also be investigated. This is shown in Fig. 6(b), where the vertical offset is measured from the center position at an optimal lateral shift. As long as one waveguide section lies within the other, an optimal coupling is observed. Thus, there is no significant reduction of the coupling efficiency when the bottom of both guides are aligned at the same height, which considerably simplifies

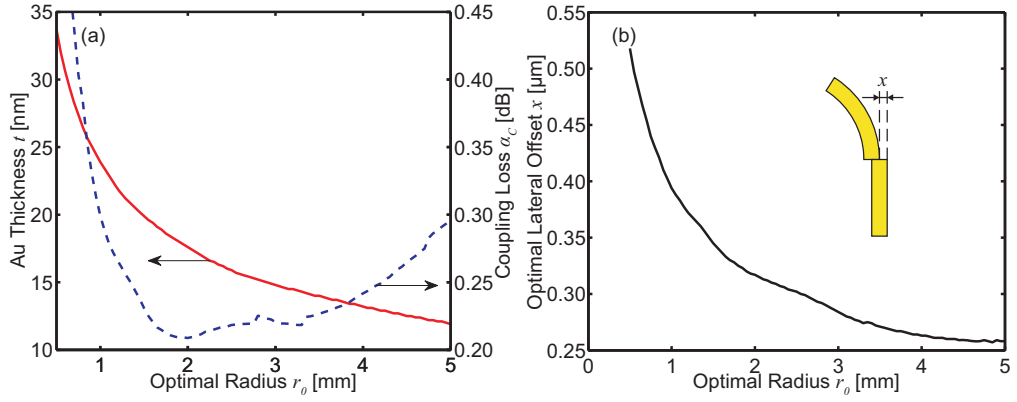

Fig. 7. Straight and optimally bent waveguide coupling: (a) Au strip thickness and coupling loss as a function of the optimal radius. (b) Optimal lateral offset as a function of the optimal radius. The Au strip is 3 µm wide.

#144920 - $15.00 USD Received 28 Mar 2011; revised 21 Aug 2011; accepted 28 Aug 2011; published 15 Sep 2011

the fabrication process.

With all optimization elements at hand, the minimal coupling loss as a function of the bending radius can now be calculated for a portion of the circuit shown in Fig. 1. Both, the straight and the curved waveguides are 3 μm wide. The thickness is 20 nm for the straight waveguide. The thickness of the curved one is such that the bending radius is optimal. For a thick Au strip, the corresponding optimal radius is small. This dependency can be seen in the solid line in Fig. 7(a) (in this figure, the origin of the small bump in the coupling loss curve around 3 μm is not clear and does not appear to be caused by the mesh used for the calculation). The dashed line in this figure corresponds to the coupling losses. The coupling losses reach their minimum when the curved waveguide has about the same thickness as the straight one since the field distributions are similar in that case. However, it should be noted that the coupling losses are about ten times smaller than the bending losses (see Fig. 5). Figure 7(b) shows the lateral offset for minimal coupling losses as a function of the bending radii. The larger the radius, the smaller the required offset.

4. Conclusion

We presented a flexible and convenient approach for the simulation of complete plasmonic circuits realized with different waveguide elements such as straight and bent waveguides. The implementation using a commercial finite element solver of different waveguide geometries — including bends — has been detailed, together with the required specific boundary conditions. This method was successfully applied to design integrated plasmonic circuits. Waveguide coupling and curvature have been optimized for minimal losses. Provided a low reflexion coupling, the losses due to the coupling are about 10 times lower than those caused by ninety degree bends. Therefore bending losses remain the most critical issue for the integration of long–range plasmonic waveguides.

Acknowledgments

Funding from the Swiss National Center of Competence in Research Nanoscale Science is gratefully acknowledged.

#144920 - $15.00 USD Received 28 Mar 2011; revised 21 Aug 2011; accepted 28 Aug 2011; published 15 Sep 2011